Proceedings of the International Gas Turbine Congress 2003 Tokyo
November 2-7, 2003

IGTC2003Tokyo TS-082

The Effects of Oblique Discrete Rib Arrangement on Heat Transfer Performance of a Square Duct

Kazuya TATSUMI[1], Hiroshi IWAI[1] and Kenjiro SUZUKI[1]

[1]Department of Mechanical Engineering
Kyoto University
Sakyo-ku, Kyoto 666-8501, JAPAN
Phone: +81-75-753-5219, FAX: +81-75-753-5251, E-mail: ktatsumi@mbd.nifty.com

ABSTRACT

Three-dimensional numerical simulation was conducted by making use of a RANS approach for the flow in a duct accompanying longitudinal vortices and discussions are given for the related thermal fields. In the first half of this paper, applicability of the three turbulence models adopted in the present study is discussed based on the comparison with published experimental results both for the flow around a rectangular winglet vortex generator and for the inclined impinging jets. The results obtained with the non-linear eddy viscosity models agree reasonably well with the experiments.

Main part of the article treats the numerical results for the flow around a discrete rib attached obliquely to the flow direction onto the bottom wall of a square duct in which a fully developed turbulent flow is established at the inlet. The rib attack angle to the main flow was varied in several levels from $\beta = 20^\circ$ to 75°. The ratio of the rib height to the duct hydraulic diameter and the duct Reynolds number were set to be $e/D = 0.15$ and $Re = 20,000$, respectively. Due to the rib inclination and the gaps existing between the rib ends and the sidewalls, a noticeable heat transfer augmentation is obtained downstream the rib where the separated flow from the leading edge of the rib reattaches. As β decreases, the region of heat transfer deterioration behind the rib is reduced in size. Furthermore, heat transfer enhancement incurred by the downwash flow and the longitudinal vortex becomes more conspicuous. Heat transfer enhanced region however becomes narrower as β decreases since the cross section of the generated longitudinal vortex becomes smaller then. Combination of the two effects produces the most effective heat transfer enhancement in the case of $\beta = 45^\circ$ among the tested cases.

NOMENCLATURE

AR	duct aspect ratio
d	jet nozzle diameter
D	hydraulic diameter
C_p	pressure loss coefficient
e	rib height, winglet height
H	duct height
k	turbulent kinetic energy
Nu	Nusselt number based on D and fluid local bulk mean temperature
P	pressure
Pr	Prandtl number
Re	Reynolds number $U_m D/\nu$
U_i	velocity components
U_m	channel mean streamwise velocity
VR	velocity ratio between the cross-flow and jet
W_D	duct width
W_r	rib width
Greek symbols	
β	angle of attack of oblique rib and winglet
Γ	circulation
θ	jet skew angle
μ	viscosity
ρ	density
ϕ	jet pitch angle
Ω_{max}	maximum vorticity
subscripts	
0	value for a smooth circular tube

Manuscript Received on March 31,2003

INTRODUCTION

Use of a rib-roughened channel is one of the basic and effective tools for the enhancement of internal flow convective heat transfer. It has been used in various industrial applications such as corrugated plate heat exchangers or serpentine cooling passages in high temperature gas turbine blades. Flow within the rib-roughened channels is highly three-dimensional especially for the cases of small aspect ratio. So the pattern of accompanying flows and the mechanism of related heat transfer strongly depend on the rib geometry. Therefore, numerous investigations have been conducted for many kinds of rib arrays in the past few decades.

A full-span rib mounted perpendicularly to the flow direction is the standard one and its friction and heat transfer characteristics have been studied first(Han et al., 1984, Acharya et al., 1997). Oblique ribs and V-shaped ribs possessing certain angle of attack have been studied next(Han et al., 1985, Fann et al., 1994, Ekkad and Han, 1997, Iacovides et al., 2001, Jang et al., 2001). Inclination of the ribs to the flow direction invokes secondary flow downstream the rib. Mixing to be incurred between the duct core region and the wall vicinity region effectively enhances the wall heat transfer (Kiml et al., 2001, Mohammad et al., 2002). Furthermore, several references demonstrate that introduction of discrete ribs, the ribs interrupted by gaps in their spanwise direction, is effective in the augmentation of heat transfer (Taslim et al., 1996,Tatsumi et al., 2002). Flow passing through the gap directly produces the enhancement of heat transfer. It also affects the pattern of recirculating flow behind the rib and reduces the size of the low efficiency region

of heat transfer (Tatsumi et al., 2002). Therefore, oblique ribs with spanwise gaps are expected to further improve the wall heat transfer in relation with the secondary flow or the longitudinal vortices to be generated (Hu et al., 1996) in addition to the shrinkage of the ineffective recirculating flow region. They may produce even a chance to reduce the pressure loss penalty (Cho et al., 2001). However, flow pattern to be produced should be complicated and must be studied in detail.

In the present article, discussion will be developed for the flow pattern to be produced around an oblique discrete rib attached onto the duct bottom wall in a fully developed turbulent flow region, based on the results of a three-dimensional numerical computation. The discussion aims at giving insight for the flow pattern and related heat transfer to be produced in a duct and at providing hints to experimentalists for future detailed study. Unfortunately, Direct Numerical Simulation is yet very difficult even with the most advanced super-computer. So, the present numerical computation adopts a RANS approach which introduces ambiguity to some extent depending on the applicability of the turbulence models to be employed. In this connection, preliminary computations were carried out for two types of flows similar to the one to be treated in the present article in a sense that longitudinal vortices are generated in a channel. One is the vortex generated with a rectangular winglet vortex generator and another is the one generated with a skewed and pitched jet injected into a cross-flow in a channel. The discussions in this part show that the present numerical computation may work for the purpose mentioned above, at least, in qualitative sense.

NUMERICAL PROCEDURE

Due to the high Reynolds number and the complicated geometrical structure of the rib treated here, adoption of Direct Numerical Simulation is impractical as a means to tackle the problem. Therefore, a RANS approach was employed in the present study by applying eddy viscosity models for solving the momentum equation. As a numerical procedure, time-dependent forms of the governing equations are solved for the following reason. For a separating and reattaching flow, such as the backward-facing step flow, separated shear layer contains large-scale vortices periodically formed and moving toward the reattachment point. This produces periodical fluctuation of velocity and other quantities and can significantly contribute to the heat transfer characteristics especially at the reattachment point (Tatsumi et al., 1999). With an approach to solve the time-dependent forms of the momentum and energy equations, effects of apparent shear stresses and heat fluxes to be produced by these large-scale vortical motions can automatically be taken into account in the computation.

Thus the governing equations solved in the present study are the following three-dimensional, incompressible, time-dependent forms of continuity, momentum and energy equations:

$$\frac{\partial U_i}{\partial x_i} = 0 \tag{1}$$

$$\frac{D\rho U_i}{Dt} = -\frac{\partial P}{\partial x_i} + \frac{\partial}{\partial x_j}\left(\mu\frac{\partial U_i}{\partial x_j} - \rho\overline{u_i' u_j'}\right) \tag{2}$$

$$\frac{D\rho\Theta}{Dt} = \frac{\partial}{\partial x_j}\left(\frac{\mu}{Pr}\frac{\partial\Theta}{\partial x_j} - \rho\overline{u_j'\theta'}\right) \tag{3}$$

The turbulence models employed here to determine the Reynolds stresses, i.e. the last term of Eq. (2), are categorized as a low Reynolds number version of eddy viscosity model. Three different models are tested in the present study, i.e. the ones proposed by Launder and Sharma (Launder and Sharma, 1974) (hereafter referred to as LS model), by Abe, Kondoh and Nagano (Abe et al., 1997) (hereafter referred to as NLAKN model) and by Craft, Launder and Suga (Craft et al., 1996) (hereafter referred to as CLS model). LS model is one of the classic models and has been tested most frequently so far by many researchers. It is simple in form and is numerically stable. NLAKN model is one of the typical non-linear eddy viscosity models and has been demonstrated to work well for various heat transfer problems. CLS model is another non-linear eddy viscosity model retaining third order terms ignored in NLAKN model and is therefore expected to work better for flows containing rotating velocity components. For the turbulent heat flux in Eq. (3), the following gradient type assumption was adopted in the present computation.

$$-\overline{u_j'\theta'} = \frac{\nu_t}{Pr_t}\frac{\partial\Theta}{\partial x_j} \tag{4}$$

where the turbulent Prandtl number, Pr_t was set to be constant and equal to 0.9. Fully implicit forms of finite-difference equivalents of the governing equations were solved numerically along the time axis in the manner adopted in reference (Iwai et al., 2000). For finite-differencing of the momentum equations, a fourth-order central difference scheme was employed for the diffusion terms while a fifth-order upwind scheme was employed for the convection terms. In the energy equation and the two governing equations for k and ε, a first-order upwind scheme was adopted for the convection terms and a central-difference scheme for the diffusion terms. The pressure gradient in the momentum equation was evaluated with the SIMPLE algorithm which solves the pressure correction so as to satisfy the finite difference equivalent of Eq. (1). Alternating direction implicit (ADI) method was employed to accelerate the conversion in iterative procedure needed to solve the elliptic-type partial differential equations.

For the winglet vortex generators and oblique ribs, in order to calculate the flow and thermal fields adjacent to the bodies with high accuracy, a composite grid system was employed in the computation. The grid system is thus composed of two different grid frames. One is the main grid system allocating the grids aligned with the duct geometric structure, i.e. the streamwise, spanwise and transverse directions. The other is a sub-grid system for which grid points are aligned with another Cartesian frame of reference rotated to match the geometry of the winglet vortex generator or oblique rib. The values of the solved quantities on each of the grid system were adjusted so as to share the common values at their overlapping boundaries at every iterative process at any time.

PRELIMINARY TEST CASES FOR TURBULENCE MODELS EMPLOYED

Here is shortly discussed some of the results obtained in the preliminary tests made for the two types of flows. These are additional cases to the results of Tatsumi et al.(2002) where the present code was compared with experiments for flow in a duct with 90° full-span ribs and discrete ribs attached onto its wall. The tested two cases are of a flow passing a rectangular vortex generator and an inclined impinging jet, respectively. Since oblique discrete ribs are believed to induce longitudinal vortices, it is essential to evaluate the applied turbulence model for such flows. Thus, these two cases are chosen as test cases additional to 90° ribs to validate the present numerical code.

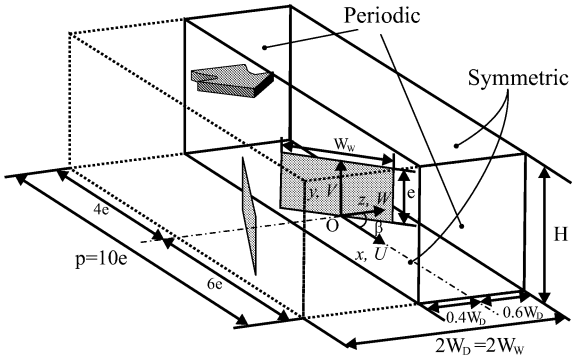

Fig.1: Computational domain of the winglet vortex generator.

Rectangular Winglet Vortex Generator

The first test flow is the one in a channel in which in-line arrays of the pairs of rectangular winglet vortex generators (hereafter referred to as WVG) are mounted to its bottom wall. The results are compared with the experiment conducted by Lau et al.(1999). Geometrical configuration of the WVG treated in the present study is shown in Figure 1 together with the adopted coordinate system. A pair of rectangular winglets, having an angle of attack and facing to each other, is attached to the duct bottom wall in a symmetric pattern. The arrays are arranged in a spatially periodical manner in both streamwise and spanwise directions. Considering these conditions for the arrangement of the WVG, periodic and symmetric boundary conditions are employed at the streamwise and spanwise boundaries, respectively. The coordinate origin is located at the center of the winglet, which is located at a distance of $4e$ from the upstream boundary. β is set to be 30°. The geometric condition of the WVG is set to be identical with the experiment of Lau et al.(1999). Reynolds number, which is based on the winglet height, is taken to be $Re = 10,000$. The turbulence models applied here in the computation are the LS model and CLS model.

Figures 2(a) and (b) illustrate the cross-sectional distributions of the streamwise velocity, U/U_m, and Reynolds stress, $\overline{u'v'}/U_m^2$, respectively. Here U_m denotes the cross sectional mean velocity in the channel. Each includes three figures and shows the values obtained at three spanwise locations of $z/W_D = -0.125$, 0.125 and 0.375 at the streamwise location of $x = -2.92e$, namely a position of $5.35e$ downstream the trailing edge of the WVG. The three spanwise locations roughly correspond to the downwash flow, the vortex center core and the upwash flow regions. The results of hot wire measurement presented by Lau et al.(1999) are depicted together in the figures. They used two types of hot wire probes in their study, i.e. a quadruple-wire probe (referred to as probe-A) and an X-probe (referred to as probe-B). Thus, the results for $\overline{u'v'}/U_m^2$ obtained with both probes are shown in Figure 2(b). Comparison of the numerical results with the experimental data plotted in the figure must be discussed with reservation giving consideration to noticeable difference existing between the two measurements.

As for the distribution of U/U_m, both models show underprediction in the center region at $z/W_D = 0.125$, a position close to the vortex core. The LS model shows a better prediction at $z/W_D = -0.125$ whereas it largely differs with the experimental data at $z/W_D = 0.375$. CLS model overpredicts the mean streamwise velocity at $z/W_D = -0.125$. However good agreement is observed at $z/W_D = 0.375$. On the whole, the present results obtained with CLS model show

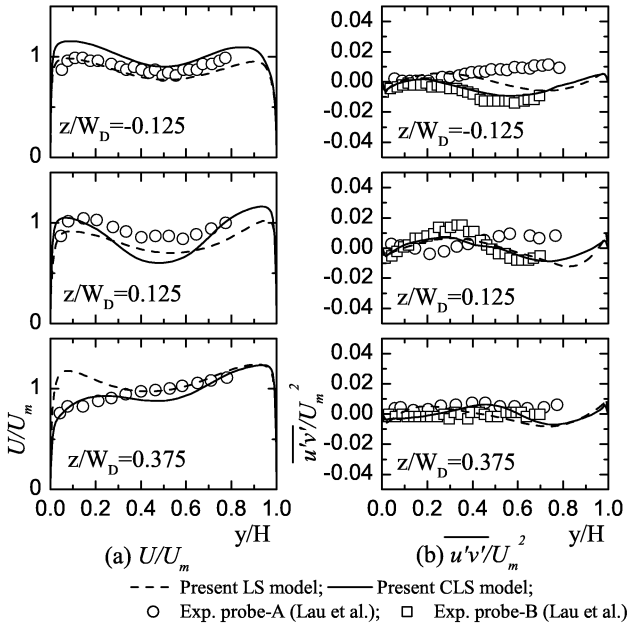

Fig.2: Transverse distributions of U/U_m, $\overline{u'v'}/U_m^2$ and $\overline{u'w'}/U_m^2$.

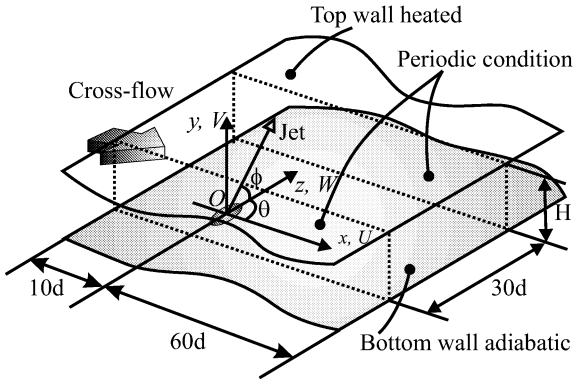

Fig.3: Computational domain of the inclined impinging jet.

a reasonable agreement with the experimental data. As for the turbulence quantities, it is noticed that CLS model shows a better performance in predicting $\overline{u'v'}/U_m^2$ values than the LS model. Additionally to be marked here, the present results of $\overline{u'v'}/U_m^2$ show better accordance with the data of probe-B, the probe of simpler geometry. Higher accuracy expected in the measurement with the probe-A may not have been achieved because of its positioning difficulty related to its complicated geometry.

Inclined Impinging Jets

The second test flow is a skewed and pitched jet injected into a cross flow in a channel. Such inclined jet is known to produce longitudinal vortex at the downstream of the jet which induces heat transfer augmentation at the channel walls. This is similar to the flow to be studied as the main target of the present study so that it is taken to be one of the test flows to study the applicability of the turbulence models. The present results are compared with the experiment carried out by Nakabe et al.(1998).

The computational domain of this case is schematically

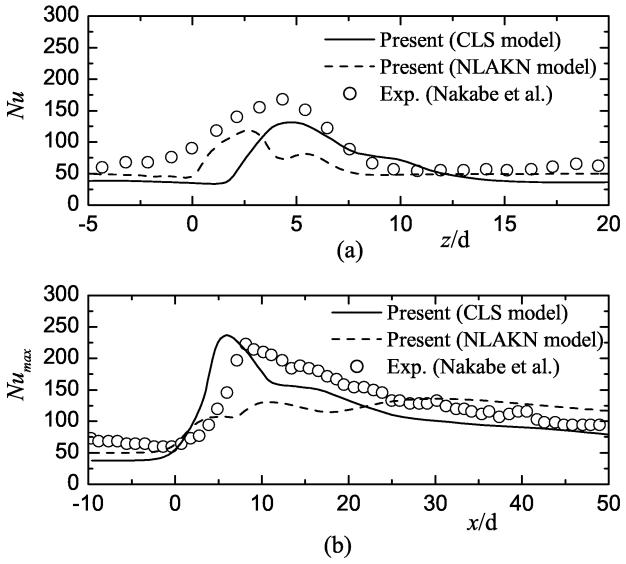

Fig.4: (a) Spanwise distribution of Nu at $x/d = 20$ and (b) streamwise distribution of peak Nusselt number, Nu_x at each streamwise position.

shown in Figure 3 together with the geometrical parameters and coordinate systems to be used here. The jet is inclined in a way characterized by two angles: the skew angle $\theta = 90^\circ$ and the pitch angle $\phi = 45^\circ$. The origin of the coordinate system is located at the center of the outlet port of the jet nozzle having elliptic shape. The inlet and outlet boundaries of the computational domain are located respectively at $x/d = -10$ and $x/d = 60$, where d is the diameter of the jet nozzle. Approaching flow to the channel inlet is hydro-dynamically taken to be a fully developed one in a channel. Periodic boundary conditions are applied at both side boundaries of the computational domain for simplicity, while in the experiments a single nozzle was mounted in a channel having the aspect ratio of 14.4. The channel height to jet diameter ratio is $H/d = 5$ and the channel domain width to jet diameter ratio is $W_D/d = 30$, respectively. The channel flow Reynolds number defined with the cross-sectional mean velocity and the channel hydraulic diameter is $Re = 5,000$. The jet to channel flow velocity ratio is set to be $VR = 3$. Although the jet Reynolds number based on the jet mean velocity and jet nozzle diameter is $Re_J = 1,500$, injected flow from the nozzle is treated in the computation to be turbulent at the nozzle outlet and the time mean velocity and other quantities are determined from the corresponding values for a fully developed turbulent flow in a circular tube. The working fluid is water but no information about the inlet flow temperature was supplied in the reference (Nakabe et al., 1998). In this computation, the Prandtl number is set to be $Pr = 6.7$. Top wall of the channel was heated in the experiments and the Nusselt number measured on the top wall inner surface is discussed here. Thermal field of the channel at the nozzle location was reported in the experiments to be still weakly developing but, in the computation, it is treated to be fully developed at constant heat flux condition for simplicity. For the turbulence models, NLAKN model and CLS model are employed in the present computation.

Figure 4(a) shows the spanwise distribution of Nusselt number, Nu, calculated at the streamwise location $x/d = 20$. The experimental results of Nakabe et al.(1998) are also displayed in the figure for comparison. Although the peak Nu is underpredicted and the calculated peak position does not precisely coincide with the experimental counterpart, both numerical results capture the essential features of the experimentally obtained distribution of Nu. Especially, the calculated result with the CLS model agrees fairly well with the experimental counterpart. The discrepancy between the calculated and experimental peak positions of Nu is to some extent produced by the spanwise flow induced more strongly by the periodic side boundary condition adopted in the computation. Lower numerical results of Nusselt number come partially from the numerical negligence of weak development of thermal field observed in the experiments at $x/d = 0.0$. It is also related to the ambiguity in the inlet flow temperature and to the possible difference between the experiments and the present calculation in the jet velocity profiles.

In Figure 4(b) is plotted the peak Nusselt number at each streamwise position, Nu_{max}, against x/d. While the numerical result with the NLAKN model is almost flat, the one with CLS model agrees fairly well with the experimental data. The first peak is caused by the jet impingement and the second peak is due to the effect of the generated longitudinal vortex.

Considering all of the points raised in the above, CLS model is judged to work reasonably well in the prediction of the thermal field affected by the generated longitudinal vortices.

RESULTS AND DISCUSSION

Discussion is now given to the flow pattern and its related heat transfer characteristics around a single rib attached with an angle of attack onto one of the walls of a duct having small aspect ratio. The adopted computational domain is illustrated in Figure 5 together with the geometric parameters and the main coordinate system where its origin is located at the duct centerline. A fully developed turbulent flow is assumed to approach the inlet boundary, which is located $10e$ upstream the rib, and the outlet boundary is located at a position $35e$ downstream the rib, where e is the rib height. The aspect ratio of the duct, AR, is set to be unity. Reynolds number based on the hydraulic diameter of the duct is fixed and is set equal to $Re = 20,000$. Rib height to duct height ratio and rib width to duct width ratio are set equal at $e/H = 0.15$ and $W_r/W_D = 0.6$, respectively, while the rib possesses a square shape cross section. The angle of attack of the rib to the main flow is varied in several steps, i.e. $\beta = 20^\circ$, 30°, 45°, 60° and 75°. Regarding the previous discussions concerning the rectangular WVG and inclined impinging jet, the CLS model is chosen here for the turbulence model applied to the computation. For wall boundaries, constant heat flux condition is applied to the duct walls and to the rib surface.

The grid number is $227 \times 57 \times 77$ for the main grid system and $36 \times 57 \times 52$ for the sub-grid system. A test for grid independency of the computation was carried out by varying the grid numbers in the three directions. Since the wall heat transfer value is most sensitive to the grid density in the normal direction of the wall, the discussion of grid dependency only in the y direction will be shown here. Three kinds of grid node variations were tested, i.e. $227 \times 52 \times 77$, $227 \times 57 \times 77$ and $227 \times 75 \times 77$ for the main grid. The values of y^+ for each grid were approximately 5, 2 and less than 1. Only one case of the angle of attack was examined, i.e. $\beta = 45^\circ$. The overall heat transfer coefficient decreased by 3.5 percent between the first two cases and there was no severe difference between the latter two cases. A grid inde-

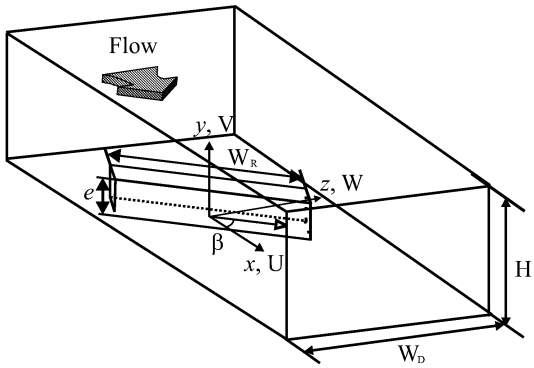

Fig.5: Computational domain of the oblique discrete rib.

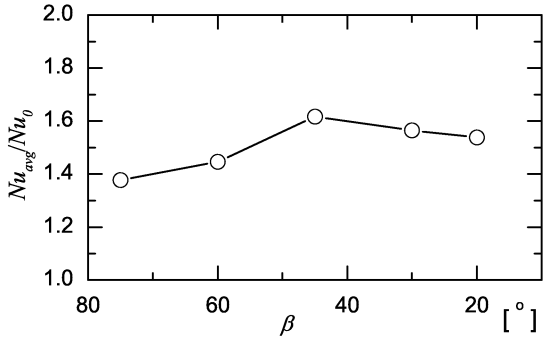

Fig.6: Spatially averaged Nusselt number, Nu_{avg}/Nu_0.

pendent study was also carried out by Suga(1998) and he has reported that the CLS model produces accurate results for $y^+ \leq 4$. From these discussions, the aforementioned grid numbers are chosen in the present study.

Mean Nusselt number, Nu_{avg}, spatially averaged over the region from $x/e = -5$ to $x/e = 20$ of the rib-attached duct wall including the rib surfaces is shown in Figure 6. The values are normalized by Nu_0, which represents the Nusselt number for a fully developed turbulent flow in a circular tube correlated by McAdams(1942) as follows:

$$Nu_0 = 0.023 Re^{0.8} Pr^{0.4} \tag{5}$$

Nu_{avg}/Nu_0 increases as the angle of attack decreases and takes a maximum peak at $\beta = 45^\circ$, and then starts to decrease with a further decrease of β. Thus, the largest heat transfer augmentation is obtained at $\beta = 45^\circ$.

Streamwise local but spanwise-averaged Nusselt number, Nu_x/Nu_0, is plotted against x/e in Figure 7(a). Rib surface area is counted as a part of the total averaging area. In all the cases, the value of Nu_x/Nu_0 is larger than unity over the whole span of the streamwise locations so that the attachment of the rib enhances the duct wall heat transfer over long streamwise distance irrespective of the value of the angle of attack. Most effective enhancement is obtained in the region $5 < x/e < 10$ in every case of different value of β. In the case of $\beta = 45^\circ$, Nu_x/Nu_0 shows largest value among the results for different value of β at any streamwise position.

Figure 7(b) shows the pressure loss coefficient, C_p, which is calculated in the following form.

$$C_p = \frac{2\Delta P}{\rho U_m^2} \tag{6}$$

where ΔP is the difference of the cross sectional mean pressure between the calculated location and $x/e = -5.0$. C_p is normalized by the value C_{p0} which represents the pressure loss coefficient of a circular tube calculated from the friction factor, f_0, correlated by Petukhov (Webb, 1994).

$$f_0 = (1.58 \ln Re - 3.28)^{-2} \tag{7}$$

C_p/C_{p0} largely increases where the rib exists and pressure recovery is observed downstream of the rib for all angles of attack. In the region of $0 \leq x/e \leq 5$, C_p/C_{p0} takes its largest value for $\beta = 75^\circ$ and 60° and then decreases as β decreases. Although the present results are for discrete ribs, this order of C_p/C_{p0} is the same as that for oblique ribs without gaps as reported by Han et al.(1985). Further downstream at $x/e = 20$ the values of C_p/C_{p0} for the different cases become

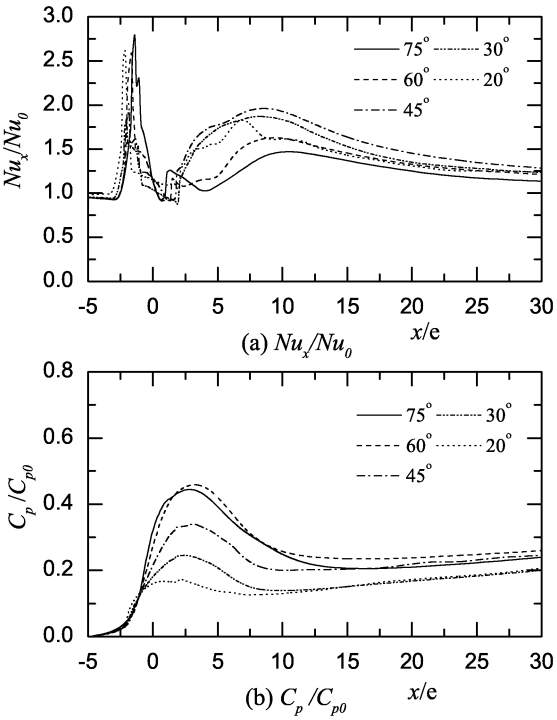

Fig.7: Streamwise distribution of (a) the spanwise-averaged Nusselt number, Nu_x/Nu_0 and (b) pressure loss coefficient, C_p/C_{p0}.

closer to each other, however, the order does not change significantly: C_p/C_{p0} is maximum for $\beta = 60^\circ$ and minimum for $\beta = 20^\circ$. Therefore, the angle of attack which produces the largest Nu_{avg} does not correspond to that of the maximum C_p/C_{p0}. These results suggest that $\beta = 45^\circ$ may be the optimum value for oblique discrete ribs in this sense.

Figure 8 shows the velocity vector maps in an x-y plane at three spanwise locations $z/W_D = -0.15$, 0.0 and 0.15 for the case of $\beta = 45^\circ$. The contour maps of the spanwise velocity, W, are superimposed on the graph, in which the shaded parts correspond to the region where W is positive. Velocity vector maps of the secondary flow in a cross section calculated at three streamwise locations $x/e = 2.0$, 5.0 and 10.0 are illustrated in Figure 9 for the case of $\beta = 45^\circ$. Figure 10 shows the spatial distribution of the local Nusselt number, Nu/Nu_0, on the rib-attached wall for various values of β. Figure 11 shows the cross-sectional distribution of the turbulent kinetic energy, k/U_m^2, calculated for various values

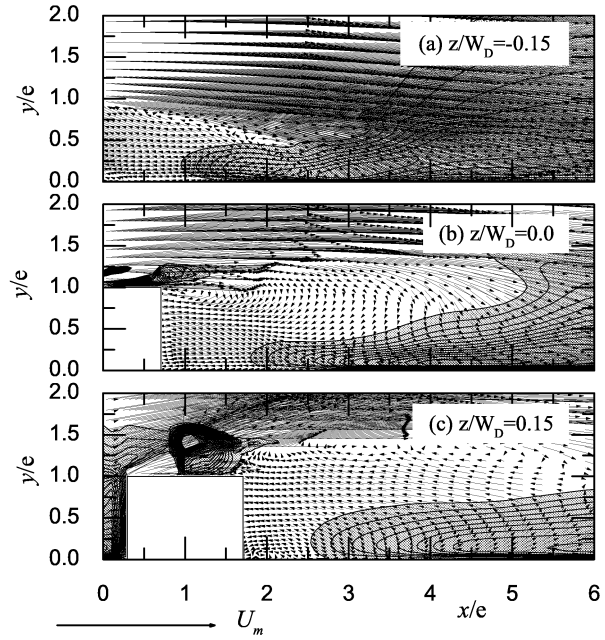

Fig.8: Velocity vectors and W contour maps at x-y cross-sectional plane ($\beta = 45°$).

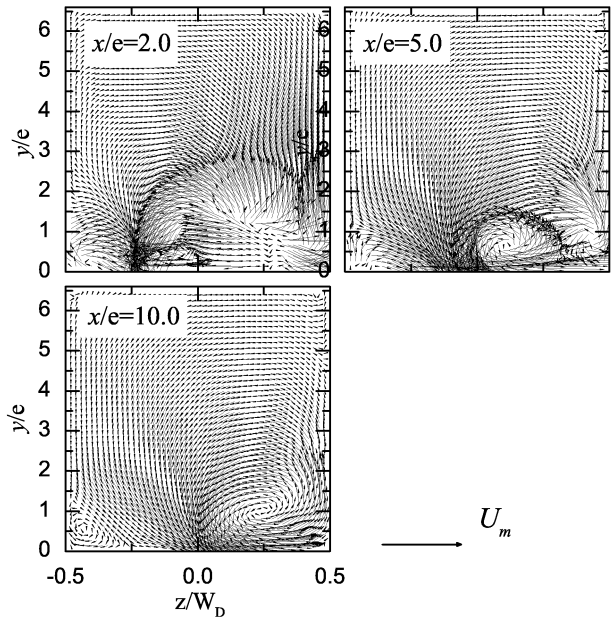

Fig.9: Velocity vectors at the y-z cross-sectional plane ($\beta = 45°$).

of β at the streamwise location $x/e = 10$ on which velocity vector maps are superimposed. In Figure 8(a), streamline of the separated flow from the rib leading edge is clearly observed to reattach the duct bottom wall. However, this is not true for Figures 8(b) and (c). As is suggested by the appearance both of the shaded and un-shaded parts near the wall in Figure 8, near wall flow has spanwise velocity or the velocity component along the rib axis in noticeable magnitude. Because of the existence of the spanwise flow near the wall, the separated flow streamline starting from the edge of the rib does not reattach at the duct bottom

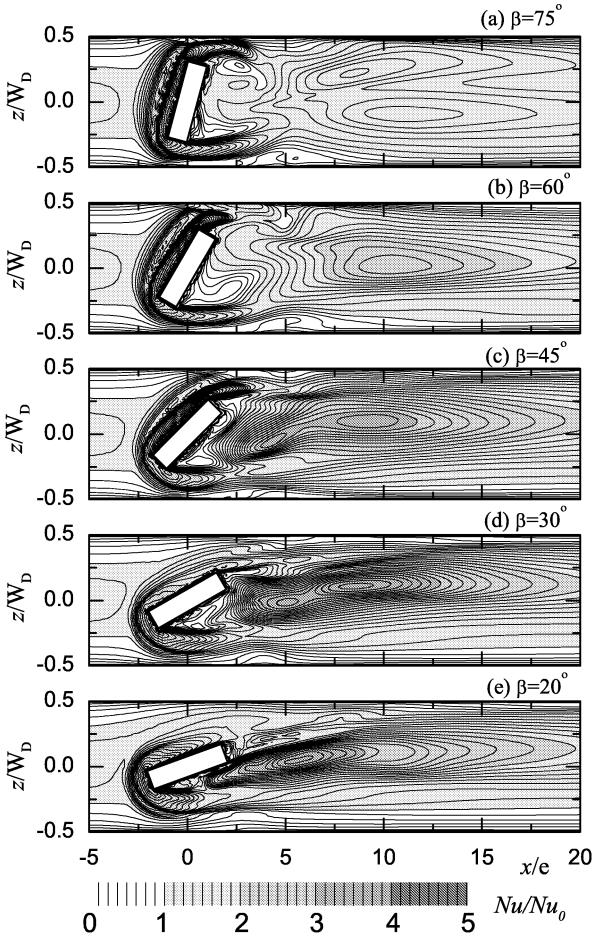

Fig.10: Nu/Nu_0 distribution on duct bottom wall.

wall at other spanwise positions as found in Figures 8(b) and (c), and is actually bifurcated into two streamlines directed upstream and downstream at a position detached from the wall. Because of this, velocity of near wall flow becomes larger with the decrease of the rib angle of attack. In the case of $\beta = 90°$, recirculating flow region appears behind the rib near the duct centerline and Nusselt number takes low value there because of small near wall flow velocity. This should be improved in the case of using the oblique discrete rib having smaller angle of attack due to the appearance of larger near wall flow velocity as discussed above.

There occurs another effect with the decrease of the rib angle of attack, which causes the change of the spatial distribution pattern of local Nusselt number. It is related to the generation of the longitudinal vortex. As is seen in Figure 9, the separated flow streamlines starting from one end of the rib located on negative side of z accompanies flow rotation as well as the above-discussed conspicuous downwash flow at $x/e = 2.0$. The rotating flow develops into a longitudinal vortex downstream slightly accompanying the deflection toward the positive z direction as is easily found in the figures for the downstream positions of $x/e = 5.0$ and $x/e = 10.0$. In the same manner as the previously discussed inclined jet case, this longitudinal vortex produces effective heat transfer augmentation at the bottom wall over large span of streamwise distance as is observed in Figure 7(a). It is reported in the reference (Tiggelbeck et al., 1991) that for delta winglet type vortex generators, a longitudinal vortex is not clearly formed for large angles of attack. Namely

Table 1. Peak vorticity and circulation at $x/e = 10$

β	75°	60°	45°	30°	20°
Ω_{max}/U_m (1/m)	-	-34.1	-31.3	-45.3	-58.1
$\Gamma/U_m \times 10^2$ (m)	-	-1.18	-1.49	-1.18	-0.821

the critical angle is reported to be $\beta_c \simeq 70°$ and no vortex was appreciable above that angle. In the present results, although not shown here, a longitudinal vortex of large scale was recognizable at $\beta \leq 60°$ resulting in larger heat transfer augmentation at the bottom wall. This gives another reason why better performance of heat transfer is obtained at $\beta = 45°$ than at $\beta = 75°$. However, on the other hand, the generated longitudinal vortex becomes slender in its cross-sectional size with the decrease of β as is estimated from the shrinkage of the cross-sectional area of high turbulent kinetic energy region shown in Figure 11. Table 1 shows the peak value of the streamwise vorticity and the circulation calculated at the location of $x/e = 10.0$ for the four cases of different value of β. The circulation is obtained by spatially integrating the streamwise vorticity in the cross section. In the integration, value smaller than 20% of the peak vorticity was not taken into account. The values are not shown here for $\beta = 75°$ since a clear vortex formation was not found for this case. From the decrease of the maximum vorticity with the decrease of the angle of attack, it is confirmed that generation of the longitudinal vortex becomes more conspicuous at smaller value of β. On the contrary, however, the largest value of the circulation is obtained at $\beta = 45°$. This suggests that the generated longitudinal vortex becomes slender with the decrease of β. Therefore, with the decrease of β, the local Nusselt number becomes larger because of the generated longitudinal vortex but the width of the heat transfer enhanced-region is reduced. These are the background why Nu_{avg} takes largest value at $\beta = 45°$. One more point to be noted here is that the level of turbulent kinetic energy is larger at larger value of β as is found in Figure 11. This indicates that a rib of larger angle of attack yields salient interruption of the main flow and therefore generates stronger turbulence. This further suggests that turbulent kinetic energy takes a minor role on heat transfer enhancement and that, at smaller value of β, more effective heat transfer is achieved with causing smaller disturbance to the flow in a duct.

Figure 12 shows the contour of the local Nusselt number, Nu/Nu_0, at the duct sidewall at $z/W_D = 0.5$ for the case of $\beta = 45°$. For a duct of small aspect ratio, as is the present case, a substantial effect to the duct sidewall heat transfer occurs. A noticeable peak of Nu/Nu_0 appearing at $x/e \simeq 5$ is caused by a vortical flow induced at the corner, which is clearly discernible in Figure 9 at $x/e = 2.0$ and $x/e = 5.0$. This vortical flow sweeps the wall surface and keeps the thermal boundary layer thinner, thereby heat transfer is enhanced there.

CONCLUDING REMARKS

Three-dimensional unsteady numerical simulations were conducted using a RANS approach for the flow in a square duct attached with an oblique discrete rib to its wall. The rib was mounted with an angle of attack to the approaching flow and side-ends were detached from the sidewalls. The rib angle of attack has been varied in several steps from $\beta = 20°$ to 70° in which the flow and heat transfer characteristics were investigated. Additional to this main discussion, other two test cases were also conducted as a means of evaluating applicability of the present numerical method to such highly

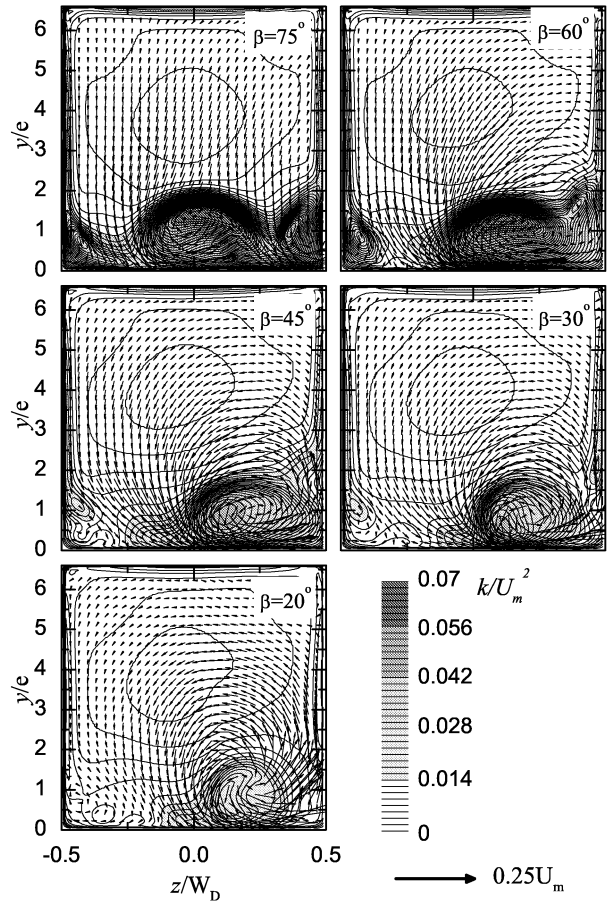

Fig.11: y-z cross-sectional view of turbulent kinetic energy contours and velocity vectors at $x/e = 10$.

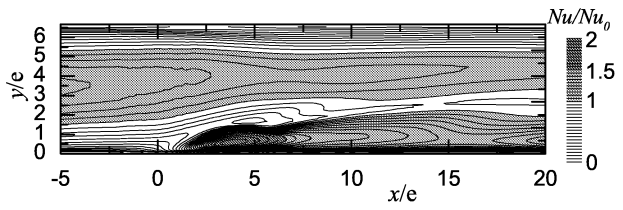

Fig.12: Nu/Nu_0 distribution on the duct sidewall ($\beta = 45°$: $z/W_D = 0.5$).

three-dimensional flows. Namely calculation was made for an array of a pair of rectangular winglets attached onto a channel wall and for a skewed and pitched impinging jet injected to a cross-flow and the obtained results were compared with experimental results. The major conclusions drawn in the discussions are as follows.

(1) Among the treated turbulence models, CLS model shows the best performance. The predicted streamwise velocity and Reynolds stresses of the rectangular winglet case and the Nusselt number of the inclined jet are in reasonable agreement with the experimental data.

(2) Oblique rib attached to a heat transfer surface produces augmentation of wall heat transfer at positions downstream the rib having the largest overall Nusselt number at the angle of attack of $\beta = 45°$. Due to the rib inclination and to the provided gaps, the flow separated from the leading edge of the rib turns its direction so as to better sweep

the heat transfer surface. This causes heat transfer augmentation at wall and also contributes to remedying the low heat transfer in the region behind the rib by reducing its size. A longitudinal vortex is generated by the rib. At rib downstream position, thinning of the thermal boundary layer is produced by this vortex on the duct bottom. This results in heat transfer augmentation there. Although larger maximum vorticity is observed for smaller value of β, the vortex becomes slender and the width of heat transfer enhanced-region is decreased. As a result of a trade-off matter of these features, the aforementioned $\beta = 45^\circ$ shows the highest heat transfer performance among the tested cases.

(3) The inclination of the rib also affects the heat transfer at the duct sidewalls. A corner vortex is generated at the trailing side-end of the rib. By the combination of this vortex and the main longitudinal vortex, a thinner thermal boundary layer is produced at one side of the duct sidewalls located at $z/W_D = 0.5$. Thus enhancement of the wall heat transfer is obtained in this area.

ACKNOWLEDGEMENTS

This article is written based on the results of the research work of the CREST project "Micro Gas Turbine and Solid Oxide Fuel Cell Hybrid Cycle for Distributed Energy System" supported by the Japan Science and Technology Corporation (JST). The article is also supported by the Japan Society for the Promotion of Science (JSPS) and the first author gratefully acknowledge the scholarship provided by them.

REFERENCES

Abe, K., Kondoh, T., and Nagano, Y., 1997, "On Reynolds-stress Expressions and Near-wall Scaling Parameters for Predicting Wall and Homogeneous Turbulent Shear Flows", Int. J. Heat and Fluid Flow, Vol. 18, pp.266-282.

Acharya, S., Myrum, T., Qiu, X., and Sinha, S., 1997, "Developing and Periodically Developed Flow, Temperature and Heat Transfer in a Ribbed Duct", Int. J. Heat Mass Transfer, Vol. 40, pp.461-479.

Cho, H. H., Lee, S. Y., and Wu, S. J., 2001, "The Combined Effects of Rib Arrangements and Discrete Ribs on Local Heat/Mass Transfer in a Square Duct", an ASME paper, 2001-GT-175.

Craft, T. J., Launder, B. E., and Suga, K., 1996, "Development and Application of a Cubic Eddy-viscosity Model of Turbulence", Int. J. Heat and Fluid Flow, Vol. 17, pp.108-115.

Ekkad, S. V., and Han, J. C., 1997, "Detailed Heat Transfer Distribution in Two-Pass Square Channels with Rib Turbulators", Int. J. Heat Mass Transfer, Vol. 40, pp. 2525-2537.

Fann, S., Yang, W-J., and Zhang, N., 1994, "Local Heat Transfer in a Rotating Serpentine Passage with Rib-Roughened Surfaces", Int. J. Heat Mass Transfer, Vol. 37, pp.217-228.

Han, J. C., 1984, "Heat Transfer and Friction in Channels with Two Opposite Rib-Roughened Walls", ASME J. Heat Transfer, Vol. 106, pp.774-781.

Han, J. C., Park, J. S., and Lei, C. K., 1985, "Heat Transfer Enhancement in Channel with Turbulence Promoters", Vol. 107, pp. 628-635.

Hu, Z., and Shen, J., 1996, "Heat Transfer Enhancement in a Converging Passage with Discrete Ribs", Int. J. Heat Mass Transfer, Vol. 39, pp.1719-1727.

Iacovides, H., Jackson, D. C., Kelemenis, G., Launder, B. E., Yuan, Y.-M., 2001, "Flow and Heat Transfer in a Rotating U-bend with 45° Ribs", Int. J. Heat and Fluid Flow, Vol. 22, pp.308-314.

Iwai, H., Nakabe, K., and Suzuki, K., 2000, "Flow and Heat Transfer Characteristics of Backward-Facing Step Laminar Flow in a Rectangular Duct", Int. J. Heat and Mass Transfer, Vol. 43, pp.457-471.

Jang, Y. J., Chen, H. C., and Han, J. C., 2001, "Computation of Flow and Heat Transfer in Two-Pass Channels with 60-degree Ribs", ASME J. Heat Transfer, Vol. 123, pp.563-575.

Kiml, R., Mochizuki, S., and Murata, A., 2001, "Effects of Rib Arrangements on Heat Transfer and Flow Behavior in a Rectangular Rib-Roughened Passage", ASME J. Heat Transfer, Vol. 123, pp.675-681.

Lau, S., Meiritz, K., and Ram, V. I. V., 1999, "Measurement of Momentum and Heat Transport in the Turbulent Channel Flow with Embedded Longitudinal Vortices", Int. J. Heat and Fluid Flow, Vol. 20, pp.128-141.

Launder, B. E., and Sharma, B. I., 1974, "Application of the Energy-Dissipation model of Turbulence to the Calculation of Flow Near a Spinning Disc, Letters in Heat and Mass Transfer", Vol. 1, pp.131-138.

McAdams, W. H., 1942, "Heat Transmission", 2nd ed., chap. 9, McGraw-Hill, New York.

Mohammad, A.-Q., Chen, H.-C., Han, J.-C.,, 2002, "A Numerical Study of Flow and Heat Transfer in Rotating Rectangular Channels (AR=4) with 45° Rib Turbulators by Reynolds Stress Turbulence Model", an ASME paper, 2002-GT-216.

Nakabe, K., Suzuki, K., Inaoka, K., Higashio, A., Acton, J. S., and Chen, W., 1998, "Generation of Longitudinal Vortices in Internal Flows with an Inclined Impinging Jet and Enhancement of Target Plate Heat Transfer", Int. J. Heat and Fluid Flow, Vol. 19, pp.573-581.

Patankar, S. V., Liu, C. H., and Sparrow, E. M., 1977, "Fully Developed Flow and Heat Transfer in Ducts Having Streamwise-Periodic Variations of Cross-Sectional Area", ASME J. of Heat Transfer, Vol. 99, pp.180-186.

Suga, K., 1998, "Recent Development in Eddy Viscosity Modeling of Turbulence", Toyota Central R&D Labs R&D Review, vol. 33, pp.39-52.

Tatsumi, K., Iwai, H., Inaoka, K., and Suzuki, K., 1999, "Prediction of Time-Mean Characteristics and Periodical Fluctuation of Velocity and Thermal Fields of Backward-Facing Step", Proc. 1st Int. Symposium on Turbulence and Shear Flow Phenomena, Santa Barbara, CA, pp.1167-1172.

Tatsumi, K., Iwai, H. and Inaoka, K., 2002, "Numerical Simulation for Heat and Fluid Characteristics of Square Duct with Discrete Rib Turbulators", Int. J. Heat Mass Transfer, Vol.45, pp.4353-4359.

Taslim, M. E., Li, T., and Kercher, D. M., 1996, "Experimental Heat Transfer and Friction in Channels Roughened with Angled, V-Shaped, and Discrete Ribs on Two Opposite Walls", ASME J. Turbomachinery, Vol. 118, pp.20-28.

Tiggelbeck, S., Mitra, N. K., and Fiebig, M., 1991, "Flow Structure and Heat Transfer in a Channel with Multiple Longitudinal Vortex Generators", Proc. 2nd World Conf. on Experimental Heat Transfer, Fluid Mechanics and Thermodynamics, Dubrovnik, pp.126-133.

Webb, R. L., 1994, "Principles of Enhanced Heat Transfer", McGraw-Hill, John Wiley & Sons, New York, chap. 2.